Lasers in Medical Science (2018) 33:1769–1779
https://doi.org/10.1007/s10103-018-2538-1

ORIGINAL ARTICLE

Evaluation of a nanocomposite of PEG-curcumin-gold nanoparticles as a near-infrared photothermal agent: an in vitro and animal model investigation

F. Rahimi-Moghaddam [1,2] · N. Azarpira [3] · N. Sattarahmady [1,2]

Received: 8 February 2018 / Accepted: 14 May 2018 / Published online: 22 May 2018

Abstract

Hyperthermia is a promising alternative modality for the conventional cancer treatments. Nanoparticle-mediated photothermal therapy (PTT) has been widely applied for hyperthermia cancer therapy by a near-infrared light irradiation. Some special nanoparticles can convert light energy into heat and destroy the tumor cells. Inspired from the photothermal efficacy of the gold nanoparticles, here we synthesized, characterized, and applied novel photothermal polyethylene glycol-curcumin-gold nanoparticles (PEG-Cur-Au NPs) in cancer PTT. The effect of PEG-Cur-Au NPs upon irradiation by an 808-nm laser on C540 (B16/F10) cell line as well as implanted (bearing) melanoma tumor in inbred C57 mice was investigated. In vitro temperature increment, cell viability evaluation, and histological analyses were performed. The results showed a dose-dependent cytotoxicity of PEG-Cur-Au NPs toward C540 (B16/F10) cell line at concentrations ≥ 25 μg mL^{-1} with an IC_{50} value of 42.7 μg mL^{-1} in dark (and with no toxicity for 10 μg mL^{-1}). On the other hand, 808-nm laser irradiation alone (without using PEG-Cur-Au NPs) for 10 min induced killing effect on the C540 (B16/F10) cell line in a laser power-dependent manner at power density > 0.5 W cm^{-2} (no toxicity for 0.5 W cm^{-2}). However, PPT using PEG-Cur-Au NPs was tremendously observed after laser illumination. Even under laser irradiation at a power density of 0.5 W cm^{-2} of PEG-Cur-Au NPs of concentrations < 10 μg mL^{-1}, PTT of the cells was substantial. Histological analyses and volume measurements of the induced tumors in the mice revealed an appropriate control of the tumors upon PTT by PEG-Cur-Au NPs. Combination of PEG-Cur-Au NP administration and 808-nm diode laser irradiation destroyed the melanoma cancer cells in the animal model.

Keywords Photothermal therapy · Melanoma cancer · Curcumin, Au, Polyethylene glycol

Introduction

Malignant melanoma is one of the most aggressive and highly metastatic skin cancers [1]. Routine treatments of cancer include surgery, radiotherapy, and chemotherapy that have risks and side effects on the normal cells, tissues, and immune system [2–4]. Compared to other conventional treatments, hyperthermia applied for eradication of tumors is a new and effective modality for the treatment of tumors. With this route, enough energy should be pumped as heat into the target tissues by irradiation of radiofrequency waves, microwave, high-intensity focused ultrasound, or laser light [5]. Either thermal or non-thermal mechanisms of cell radiation lead to irreversible changes in the structure, function, and conformation of cell membranes or macromolecules [6]. In phototherapy, there are two approaches of photodynamic and photothermal (PTT) therapies. PTT is a selective and modal therapy that can cause irreversible damage to cancer cells through heat generation by light absorption of a PTT agent [7]. A near-infrared (NIR) source supplies photons in wavelengths in a range of 700–900 nm in a way that the blood and tissue components are transparent up to 10 cm [8]. It is minimally invasive for ablation of cancer cells [9], and satisfaction of patient with cancer from PTT as compared to other

✉ N. Sattarahmady
sattarahmady@yahoo.com; nsattar@sums.ac.ir

[1] Department of Medical Physics, School of Medicine, Shiraz University of Medical Sciences, Shiraz, Iran

[2] Nanomedicine and Nanobiology Research Center, Shiraz University of Medical Sciences, Shiraz, Iran

[3] Transplant Research Center, Shiraz University of Medical Sciences, Shiraz, Iran

procedures is due to its simple procedure, quick recovery and healing, and low complications [10].

In nanoparticle-mediated PTT, nanoparticles transduce photonic energy of a NIR radiation into thermal energy [4]. Up to now, different nanostructures such as gold [11], carbon [5], silver [12], silica [13], copper [14], palladium [15], and carbon [16] based nanomaterials have been examined as appropriate agents for PTT. However, developing nanostructures with more biocompatibility, limited collateral damage, and high photoconversion efficiency still remains as an attractive issue for researchers.

Among different kinds of metal nanoparticles, gold-based nanostructures have great importance in nanobiomedicine due to low toxicity, biocompatibility, tunable surface plasmon resonance (SPR), oxidation resistance, easy surface modification, high plasmonic photothermal activity, and allocated promising therapeutic opportunities [17, 18], and they have been investigated for approval in clinical trials [19]. Gold nanostructures have been applied in numerous studies of cancer diagnostics [20], intracellular imaging [21], biological sensing [22, 23], drug and gene delivery [24], and PTT [25]. As a photothermal agent, gold nanostructures with different shapes and gold-based nanoconjugates with varying coating compounds [17, 25, 26] have been reported.

SPR arises after excitation of a metal surface at the resonance frequency and collective oscillation of the surface conductive electrons. It depends on the type, shape, and dielectric constant of nanomaterials and environmental conditions [27, 28]. Modification of the surface of gold nanostructures leads to changes in the SPR properties, e.g., red shift (shift to the higher wavelengths) in the characteristic SPR peak; this is desirable for PTT [17]. On the other hand, conjugation of gold nanostructures with biological materials induces more effective treatment of tumor cells by PTT [29].

Coating with polyethylene glycol (PEG) is desirable in the PTT of gold nanoparticles (GNPs) [30]. PEG enhances biocompatibility and stability of nanoparticles and increases their blood retention time and accumulation in the tumor site [30]. In a study, laser-stimulated PEGylated gold nanosemicubes decreased the volume of the skin tumors along with reduction of the inflammatory mediators and angiogenesis [31]. Another study showed that chitosan-modified gold nanorods were very safe and suitable for PTT with a rapid clearance and small half-life both in vitro and in vivo [32].

Curcumin is medically used due to its anti-inflammatory [33], antitumoral [34], antioxidant, antifungal [33], and antimicrobial properties [35, 36]. Antitumor activities have been reported for curcumin toward different tumor cell lines through an apoptotic mechanism [37–40]. In addition, it has a UV-vis absorption at 300–500 nm causing applications in photobiology [41]. Studies showed potential applications of curcumin in photodynamic therapy [36, 41–43]. On the other hand, conjugation of curcumin with GNPs improved its antioxidant activity [44], increased blood compatibility [45], prevented amyloid fibrillation formation [46], and enhanced bioavailability [47]. Curcumin can also be a reducing agent for GNP formation [45].

In this study, a conjugate of PEG-curcumin-gold nanoparticles (PEG-Cur-Au NPs) with NIR absorption of ~ 800 nm was designed and synthesized. Then, PEG-Cur-Au NPs were applied for PTT of C540 (B16/F10) cell line and implanted melanoma tumor in c57 mice by a continuous-wave diode laser of 808 nm as a light source. In vitro temperature increment, cell viability evaluation, and histological analyses were performed. PEG-Cur-Au NPs may offer a new and efficient photothermal treatment of cancer, after more extensive studies.

Materials and methods

Materials

All chemicals were obtained from Sigma Chemicals Co. (USA), Scharlau Chemie Co. (Spain), or Merck Co. (Germany), and used without further purification. Before use, all glassware was washed with fresh aqua regia and then deionized (DI) water. DI water was used throughout the study.

Synthesis and characterization of PEG-Cur-Au NPs

PEG-Cur-Au NPs were synthesized by chemical reduction of gold ions by PEG/curcumin. Curcumin (0.04 g) was mixed with 1.0 mL PEG (of 600 g mol^{-1} of molecular weight) and stirred for 20 min. It was then added dropwise to a stirred and boiled $HAuCl_4$ solution of 68 mg mL^{-1}, and stirring was continued for additional 10 min. The mixture was left to cool down to ambient temperature. The size and surface morphology of PEG-Cur-Au NPs were evaluated by field emission scanning electron microscopy (FESEM), using a TESCAN Mira 3-XMU (Czech Republic). UV-vis spectra were recorded by a spectrophotometer Rayleigh 2100 (China).

Evaluation of photothermal effect of PEG-Cur-Au NPs

A digital thermometer with an accuracy of 0.1 °C was employed for measurements of temperature changes upon laser irradiation into PEG-Cur-Au NPs. Different concentrations of PEG-Cur-Au NPs (2260 and 22,600 μg mL^{-1}) in autoclavable 1.5-mL plastic vials were irradiated by an 808-nm diode laser of 1.0 W with a 3.5-mm-diameter spot and 2 A supply current from DAJ Co. (Iran). Diode laser was calibrated by an optical power meter of Lambda (Australia). Output power density of irradiation was set at 1.0 W cm^{-2} by adjusting the spot size. This is accomplished through varying the distance between the output mounting lens and the target.

Temperature of PEG-Cur-Au NP-containing samples was measured every 5 min over a period of 15 min. The thermometer probe was put in the sample vials in a manner that it measured the bulk temperature of the samples without direct laser light incoming. PEG dissolved in water was used as a control at the same conditions. Each measurement was repeated thrice.

Preparations of the cells and mice

Mouse malignant melanoma cell line C540 (B16/F10) was obtained from National Cell Bank of Iran (NCBI) affiliated to Pasteur Institute of Iran (http://ncbi.pasteur.ac.ir/). The cells were cultured in Roswell Park Memorial Institute-1640 (RPMI) medium supplemented with 10% fetal bovine serum and 1% penicillin-streptomycin in a humidified cell culture incubator of 5% CO_2 at 37 °C.

Sixteen male C57/inbred mice (7 weeks old, body weight of ~ 25 g) were obtained from the Center of Comparative and Experimental Medicine, Shiraz University of Medical Sciences. The protocol was approved by the ethics committee of Animal Experiments of Shiraz University of Medical Sciences. The animals were housed in special cages at a controlled temperature (24 ± 2 °C) and humidity (40–70%) with weekly floor exchange. They had free access to water and standard pelleted laboratory animal diets. A 12:12 light/dark cycle was followed in the mentioned animal vivarium.

Evaluation of cytotoxicity of PEG-Cur-Au NPs

To examine the in vitro cytotoxicity of PEG-Cur-Au NPs, C540 (B16/F10) cells at a density of 1.5×10^4 cells $well^{-1}$ were seeded into 96-well culture plates and grew overnight. Then, the cells were incubated in the presence of different concentrations of PEG-Cur-Au NPs (5, 10 and 25, 100, 500, 1000, and 22,600 μg mL^{-1}). Cytotoxicity effect of the nanoparticles was evaluated by the MTT (3-(4,5-dimethylthiazol-2-yl)-2,5-diphenyl-tetrazolium bromide) assay after 24 h of incubation in the presence of different concentrations of PEG-Cur-Au NPs. For this purpose, the culture medium of each well was washed three times with 100 mmol L^{-1} phosphate-buffered saline (PBS), replaced by a MTT solution (100 μL of 0.5 mg mL^{-1} dissolved in PBS), and incubated in dark for 4 h at 37 °C. Then, it was centrifuged at 800 rpm for 10 min, and the supernatant was removed. The pellet was added into 100 μL dimethyl sulfoxide (DMSO) to dissolve the MTT formazan crystals. The optical density (OD) of each well was recorded at 570 nm using a microplate reader of Stat Fax (USA). Cells without treatment with the nanoparticles were used as a control. Cell viability was expressed as the ratio of the absorbance of the treated and control wells. All measurements were performed in triplicate. The half maximal inhibitory concentration (IC_{50}) was calculated from the sigmoidal curves of dose-response.

Evaluation of photothermal effect of PEG-Cur-Au NPs on C540 (B16/F10) cells

In vitro photothermal effect of PEG-Cur-Au NPs on C540 (B16/F10) cells was followed by the MTT assay. After 24 h post-seeding, C540 (B16/F10) cells in 96-well culture plates (1.5×10^4 cells $well^{-1}$) were categorized in the following groups:

(i) $L^-N^-_{cell}$ as the untreated (control) group. The cells treated with neither diode laser nor PEG-Cur-Au NPs.

(ii) $L^+N^-_{cell}$ as treated cells only with different power densities of 808-nm diode laser irradiation for 10 min. The cells were firstly incubated with the cell culture medium for 4 h and then treated with laser irradiation at different power densities of 0.5, 0.7, 1, and 1.5 W cm^{-2}.

(iii) $L^-N^+_{cell}$ as treated cells only with different concentrations of PEG-Cur-Au NPs. The cells were incubated with PEG-Cur-Au NPs of different concentrations of 5, 10, 25, 50, 100, 250, 500, 1000, and 22,600 μg mL^{-1} for 4 h. Then, the cells were kept in the dark for 10 min.

(iv) $L^+N^+_{cell}$ as the cells that were firstly incubated with PEG-Cur-Au NPs of different concentrations and then treated with different power densities of 808-nm diode laser irradiation for 10 min. At the power density of 0.5 W cm^{-2}, the cells were exposed to PEG-Cur-Au NP concentrations of 5, 10, 25, 50, 100, 250, and 500 μg mL^{-1} for 4 h. At the power densities of 0.7, 1.0, and 1.5 W cm^{-2}, the cells were exposed to PEG-Cur-Au NP concentrations of 25, 50, 100, 250, 500, 1000, and 22,600 μg mL^{-1} for 4 h.

All the groups were then incubated for 20 h at 37 °C and 5% CO_2 atmosphere and then washed three times with PBS. Cell viability was finally evaluated by the MTT assay. Cell viability was calculated as the ratio of the absorbance of the treated and control cells. All measurements were performed in triplicate.

Statistical analyses

At least three parallel experiments were conducted for each sample. Non-parametric *t* test was used to analyze the statistical significance of the results using GraphPad software. A *p* value of less than 0.05 was considered statistically significant.

Tumor implantation and photothermal therapy of tumor model in mice

The melanoma tumors were implanted by subcutaneous injection of 1.5×10^6 C540 (B16/F10) cells in 100 μL phosphate-buffered saline into subaxillary of male C57/inbred mice. Approximately 2 weeks after the tumor cell injection, solid tumors appeared. Sixteen melanoma tumor-implanted mice with an average tumor volume of about 0.55 cm^3 were selected for treatment and randomly separated into four groups. Before treatment, all the subjects were anesthetized with intramuscular injection mixture of ketamin (10%) and xylazine (2%), and shaved in the tumor areas.

The animals were categorized in the following four members of tumor-bearing mice groups: $L^-N^-_{mouse}$ as untreated (control) group including treated mice with injection of 200 μL saline, $L^+N^-_{mouse}$ as treated mice with laser irradiation of 1.5 W cm^{-2} for 10 min and intratumoral injection of 200 μL saline, $L^-N^+_{mouse}$ as the mice treated only with intratumoral injection of PEG-Cur-Au NPs, and $L^+N^+_{mouse}$ as treated mice that were firstly incubated with PEG-Cur-Au NPs for 4 h and then treated with laser irradiation. For the N^+_{mouse} groups, 200 μL PEG-Cur-Au NP dispersion in water of 2.5 mg mL^{-1} was intratumorally injected to the animals corresponding to a dosage of 25 mg kg^{-1} $mouse^{-1}$. For the L^+_{mouse} groups, the animals were exposed to 808-nm laser irradiation at a power density of 1.5 W cm^{-2} for 10 min. For the L^+_{mouse} groups, the animals were kept in the dark for 10 min. Before and after treatments, the tumor dimensions were measured by a caliper, and the tumor volume was estimated as $(a \times b^2) / 2$, where a and b were the longest and shortest diameter (mm) of the tumor site, respectively [48].

The overall health conditions of the mice before and after treatments were considered. After 48 h, all the subjects were sacrificed, and the tumoral mass and tissues of the liver, kidney, and spleen were removed for histological analyses.

Histological analyses of tumor tissues

The removed tumor tissues were fixed in 10% buffered formalin, routinely processed, and embedded in paraffin. Sections with 3–5 μm were prepared and analyzed after hematoxylin and eosin (H&E) staining. After preparation of the slides from tumor tissues, the necrotic surface areas were estimated by measuring the graticules using an Olympus microscope (Japan) in the subjects of the four groups. The percentage of necrosis (with a ×40 magnification) against the whole tumor area was estimated and graded as grade 1 (+ 1), minimal (< 10%); grade 2 (+ 2), mild (11–20%); grade 3 (+ 3), moderate (21–40%); and grade 4 (+ 4), marked (41–100%).

Inductively coupled plasma optical emission spectrometry

To determine the uptake level of the nanoparticles by the tumor cells, the gold content of PEG-Cur-Au NP-treated tumors was determined by ICP-OES using 730-ES, Varian (USA) in peak hopping gas mode. The instrument was set with the nebulizer flow of 750 mL min^{-1}. The radiofrequency power was adjusted to 1200 W, and the flow rates of the plasma gas and auxiliary gas were 15.0 and 1.50 L min^{-1}, respectively. The cellular uptake of PEG-Cur-Au NPs was determined as the quantity of gold content within the tumor, compared to the control mice (L^-N^+ group, compare to L^-N^- group).

Results and discussion

Over the past several decades, the incidence of melanoma has almost reached epidemic proportion. Late-stage melanoma is not curable by current clinical tools [49]. Therefore, hyperthermia has a potential to treat this type of cancer in some stages. On the other hand, the antitumor activity of materials such as curcumin can be simultaneously enjoyed. Besides, PEG can play a biocompatible adjustment agent. Both curcumin and PEG are also reducing agents. Therefore, PEG-Cur-Au NPs were synthesized, characterized, and employed here.

A FESEM image of PEG-Cur-Au NPs is shown in Fig. 1a. It shows that the synthesized PEG-Cur-Au NPs had a spherical shape with a mean diameter of 15.6 ± 3.2 nm. For the synthesis, both curcumin and PEG, as phenol- and alcohol-bearing functional groups, respectively, have a potential to reduce auric ions. At the same time, PEG can protect, stabilize, and embrace curcumin-GNPs to produce a conjugate of PEG-curcumin-GNPs. Figure 1b shows typical visible spectrum of PEG-Cur-Au NPs representing a SPR wavelength of ~ 536 nm and absorbance of light of 808 nm of ~ 0.1.

To evaluate the photothermal efficiency of PEG-Cur-Au NPs, their temperature increment at two concentrations of 2.26 and 22.6 mg mL^{-1} was measured under 808-nm irradiation at a power density of 1 W cm^{-2} for 15 min. Figure 2 shows the obtained results, indicating a temperature increment of 9.05 °C for the control and 18.26 and 19.45 °C for 2.26 and 22.6 mg mL^{-1} of PEG-Cur-Au NPs, respectively. Therefore, PEG-Cur-Au NPs exhibited an intense photothermal effect under 808-nm light irradiation. Because temperature increment by 2.26 mg mL^{-1} of PEG-Cur-Au NPs is enough for the PPT of cancer [50], the lower concentration was selected to avoid probable cytotoxicity of PEG-Cur-Au NPs for further in vitro and in vivo studies.

To inspect the photothermal property of PEG-Cur-Au NPs in vitro, cell viability was measured upon treatment of the C540 (B16/F10) cells with PEG-Cur-Au NPs, laser

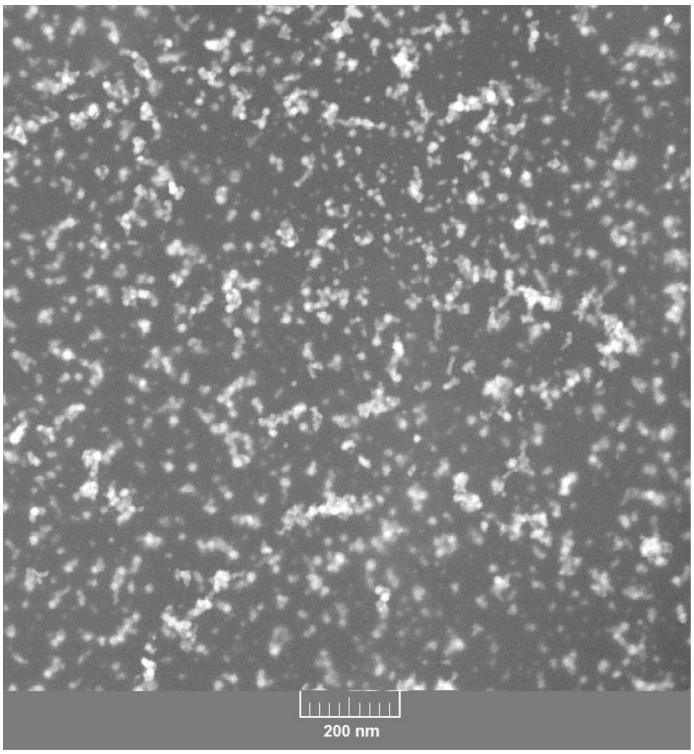

(A)

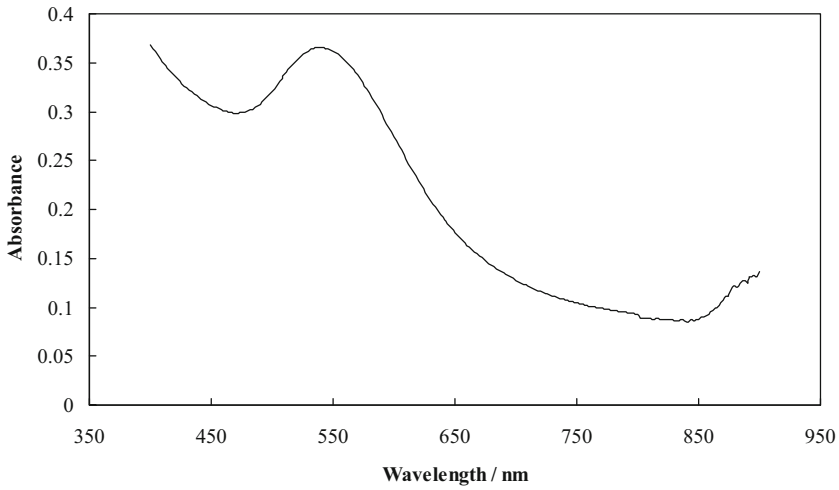

(B)

Fig. 1 A FESEM image of PEG-Cur-Au NPs (**a**) and typical visible spectrum of PEG-Cur-Au NPs (**b**)

irradiation, and the nanoparticles accompanied by the laser irradiation. Firstly, the cytotoxicity of PEG-Cur-Au NPs was investigated by seeding the C540 (B16/F10) cells in the presence of different concentrations of PEG-Cur-Au NPs (without laser irradiation) for 24 h, and measurement of cell viability was conducted using the MTT assay. Figure 3a shows the treated cells' viability compared to untreated cells showing decrement in the cell viability along with increase in the PEG-Cur-Au NP concentration in a dose-dependent manner. Here, with a PEG-Cur-Au NP concentration of 2260 μg mL^{-1}, the cell viability was decreased to 17%, and concentrations less than 10 μg mL^{-1} were relatively non-toxic, as the cell viability remained ≥ 85%. An IC_{50} value for PEG-Cur-Au NPs toward the C540 (B16/F10) cells was obtained as 42.7 μg mL^{-1}. It has been reported that curcumin with a concentration of 11.1–22.1 mg mL^{-1} (30–60 μmol L^{-1}) can induce toxicity and apoptosis in human melanoma cells after 24 h [51]. One of the reasons for this improved cytotoxicity can be enhancement in the solubility of curcumin by designing PEG-Cur-Au NPs, and this improvement was achieved by both PEG and GNPs. It was shown that arrangement of curcumin-capped GNPs enhanced water solubility of

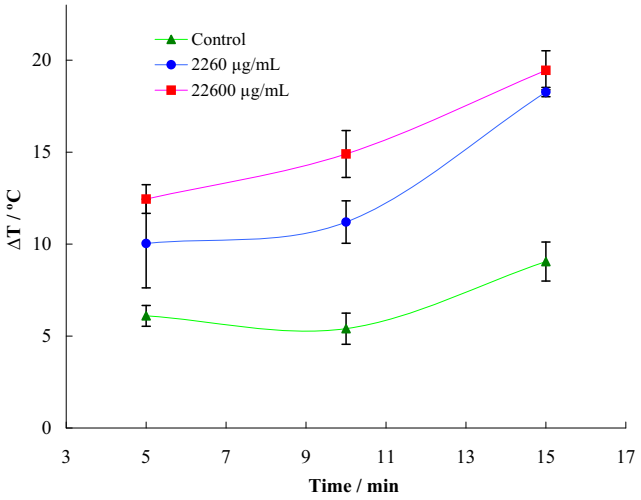

Fig. 2 Temperature increase for PEG-Cur-Au NPs with concentrations of 2260 and 22,600 μg mL^{-1} and a control sample. All the samples were exposed to a 808-nm diode laser at 1.0 W cm^{-2} for 15 min

curcumin with good antioxidant activity [44, 52]. Enhancement in the solubility of curcumin was also reported by hyaluronic acid in hyaluronic acid-curcumin-gold nanoparticles [45]. This led to enhancement of the cytotoxicity of these nanoparticles toward HeLa cells, glyoma cells, and Caco 2 cells accompanied by significant internalization into the cells [45]. Secondly, toxicity effect of 808-nm light irradiation on the C540 (B16/F10) cells was evaluated. For this purpose, C540 (B16/F10) cells were irradiated with a 808-nm laser diode at different power densities for 10 min; then, they were incubated for 24 h subsequently by cell viability evaluation by the MTT assay (relative to the untreated cells). Figure 3b shows the results of the treated cells' viability compared to untreated cells, showing that laser irradiation with a power density of 0.5 W cm^{-2} had no toxicity on C540 (B16/F10) cells (100% viability), while higher power densities did so. Statistical analyses showed significant differences between the viability values of the cells irradiate with different power densities of laser (> 0.5 W cm^{-2}) and the untreated cells ($p < 0.05$). Therefore, higher power densities of light irradiation decreased the cell viability and had a toxicity effect on the cells. Thirdly, C540 (B16/F10) cells were incubated with different concentrations of PEG-Cur-Au NPs (5–500 μg mL^{-1}) for 4 h. Then, these samples were exposed to 808-nm laser irradiation with a power density of 0.5 W cm^{-2} for 10 min. Next, the cells were rinsed several times with PBS to remove the excess nanoparticles and resuspended in PBS, and the cells' viability was measured by the MTT assay. Figure 3c shows the obtained results indicating that the viability of $L^{+}N^{+}_{cell}$ group was lower than the $L^{-}N^{+}_{cell}$ related to the more efficiency of the corresponding treatment. The differences between the cell viabilities between two groups of $L^{+}N^{+}_{cell}$ and $L^{-}N^{+}_{cell}$ for the concentrations of 5 and 500 μg mL^{-1} of PEG-Cur-Au NPs were 12 and 1%, respectively. The lower

Fig. 3 Percentage of the C540 (B16/F10) cell viability. **a** After treatment with different concentrations of PEG-Cur-Au NPs of 5, 10, 25, 50, 100, 250, 500, 1000, and 2260 μg mL^{-1}. **b** After irradiation for 10 min with 808-nm laser diode at different power densities of 0, 0.5, 0.7, 1.0, and 1.5 W cm^{-2}. **c** After 4-h incubation with different concentrations of PEG-Cur-Au NPs of 0, 5, 10, 25, 50, 100, 250, and 500 μg mL^{-1} following by irradiation for 10 min with 808-nm laser diode at a power density of 0.5 W cm^{-2}. **d** After 4-h incubation with different concentrations of PEG-Cur-Au NPs of 25, 50, 100, 250, 500, 1000, and 2260 μg mL^{-1} following by irradiation for 10 min with 808-nm laser diode at a power densities of 0, 0.7, 1.0, or 1.5 W cm^{-2}

difference in the cell viabilities obtained for the highest concentration was related to the fact that at this high concentration, PEG-Cur-Au NPs represented a high toxicity itself (in dark, without laser irradiation), and this toxicity effect covered the effect of laser light of 0.5 W cm^{-2} of power density. The obtained results indicated the power of PEG-Cur-Au NPs for photothermal application. Furthermore, the power density of laser irradiation was extended, and the cell viability of the treated cells with different concentrations of PEG-Cur-Au NPs was evaluated. The results are presented in Fig. 3d. The cell viability in the $L^{+}N^{+}_{cell}$ group at both the highest PEG-Cur-Au NP concentration and power density of laser was 9% lower than the $L^{-}N^{+}_{cell}$ group. These results are evidence of increased cell mortality following photothermal treatment by PEG-Cur-Au NPs. Curcumin can act as a photodynamic agent upon irradiation with different wavelengths of light [35, 36, 40, 51, 53]. A concentration of 25 μmol L^{-1} of curcumin shows a cytotoxic effect on AMC-HN3 cells upon irradiation at 630 nm [40]; an enhanced cytotoxicity of curcumin toward breast cancer cells was observed by 435.8-nm laser irradiation [53], and photodynamic therapy effect of curcumin was reported against methicillin-resistant *Staphylococcus aureus* upon 400–500-nm laser irradiation [35, 36]. On the other hand, GNPs represent photothermal effect with strong absorption visible to NIR lights due to SPR property. The size, shape, and dielectric constant of the medium greatly affect the SPR frequency. Increasing the size of GNP due to assemblies, aggregation, surface modification, and conjugation with other compounds induces red shift of SPR absorption toward NIR region. Link and El-Sayed (2000) investigated the PTT of GNPs using femtosecond transient absorption spectroscopy, showing that light excitation of electrons formed the heated gas. Subsequently, this converted energy is dissipated by rapid cooling of nanoparticle lattice, photon-photon interaction, and subsequently exchanging and delivering energy to local medium [54]. Local heating of the tumor environment leads to irreversible cell damage. Also, studies showed irradiation of assembly of gold nanoparticles with short laser pulses, evaporation of a thin layer of fluid around each nanoparticle, and induction of bubble formation in human breast cancer cells which led to mechanical stress and cell killing [55, 56]. Therefore, GNPs in PEG-Cur-Au NPs photothermally induce

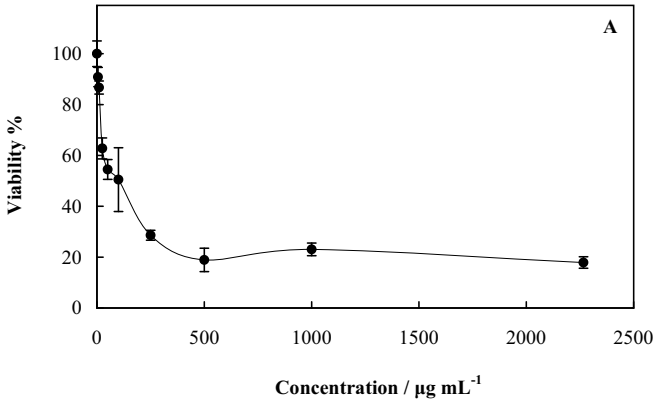
A
Viability %
100
80
60
40
20
0
0
500
1000
1500
2000
2500
Concentration / μg mL-1

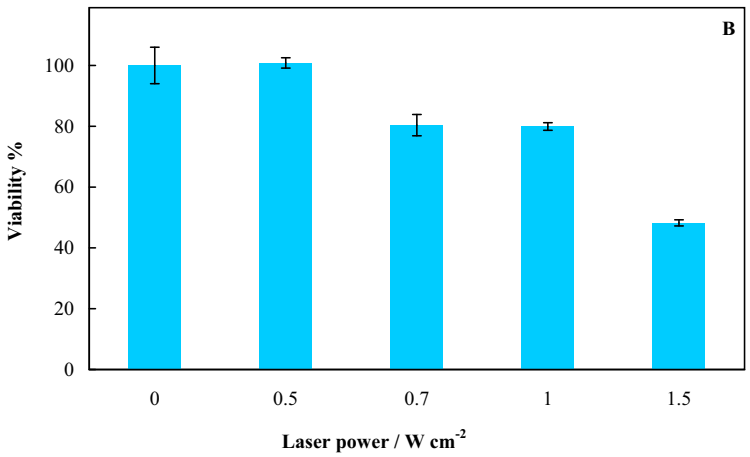
B
Viability %
100
80
60
40
20
0
0
0.5
0.7
1
1.5
Laser power / W cm-2

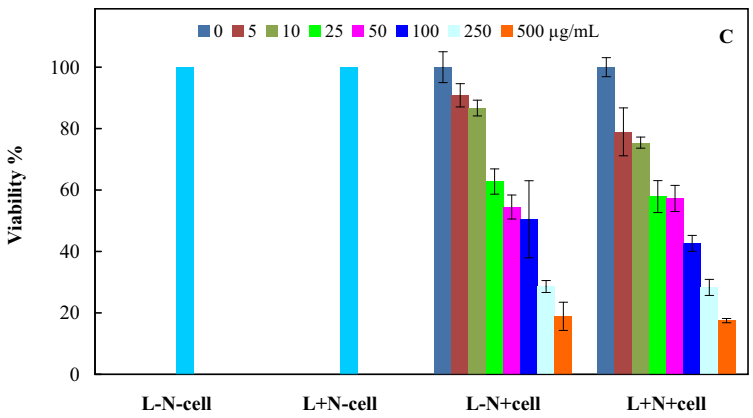
C
0 5 10 25 50 100 250 500 μg/mL
Viability %
100
80
60
40
20
0
L-N-cell
L+N-cell
L-N+cell
L+N+cell

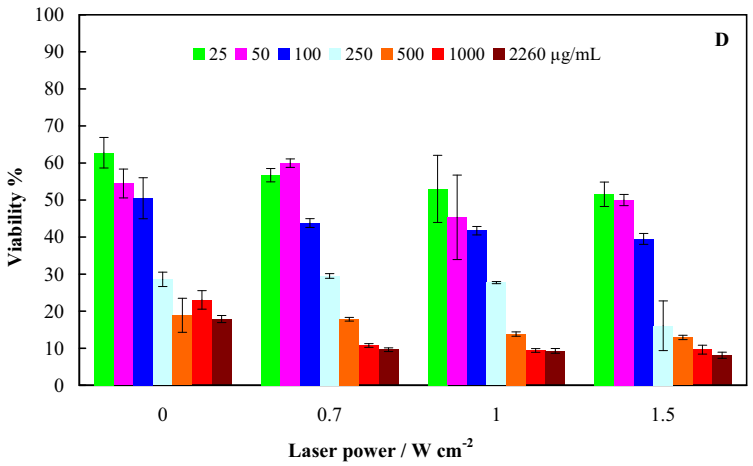
D
25 50 100 250 500 1000 2260 μg/mL
Viability %
100
90
80
70
60
50
40
30
20
10
0
0
0.7
1
1.5
Laser power / W cm-2

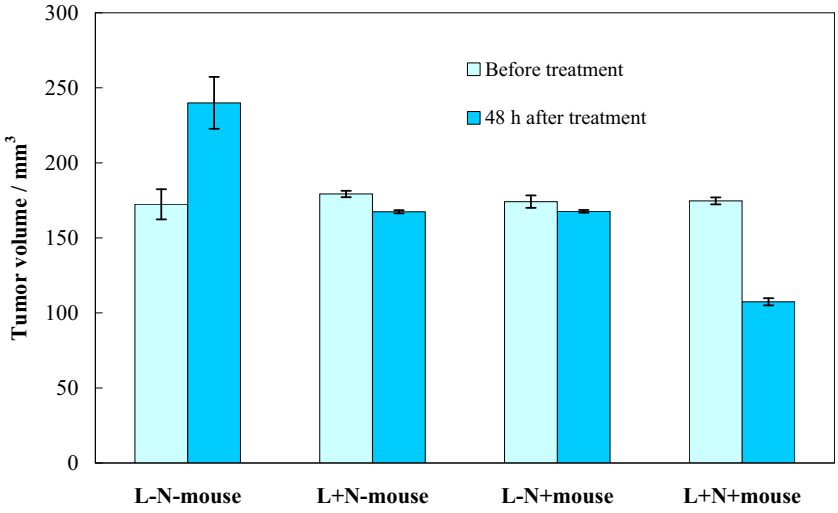

Fig. 4 Tumor volume before and after 48-h treatment for the melanoma-bearing mice in different groups of $L^{-}N^{-}_{mouse}$, $L^{+}N^{-}_{mouse}$, $L^{-}N^{+}_{mouse}$, and $L^{+}N^{+}_{mouse}$ groups

cytotoxicity. Simple bio-functionalization of GNP makes it a favorable candidate for PTT. Poor stability and biocompatibility of citrate-capped gold nanospheres were improved with PEG [57]. PEGylated nanoparticles lead to enhanced permeability and retention effect in tumors [58]. In addition, leakage feature of blood vessels and lymphatics decreasing in the tumor tissue is retained and slows the clearance of nanoparticles [58].

In order to investigate the in vitro photothermal outcomes, the localized influence of photothermal treatment on

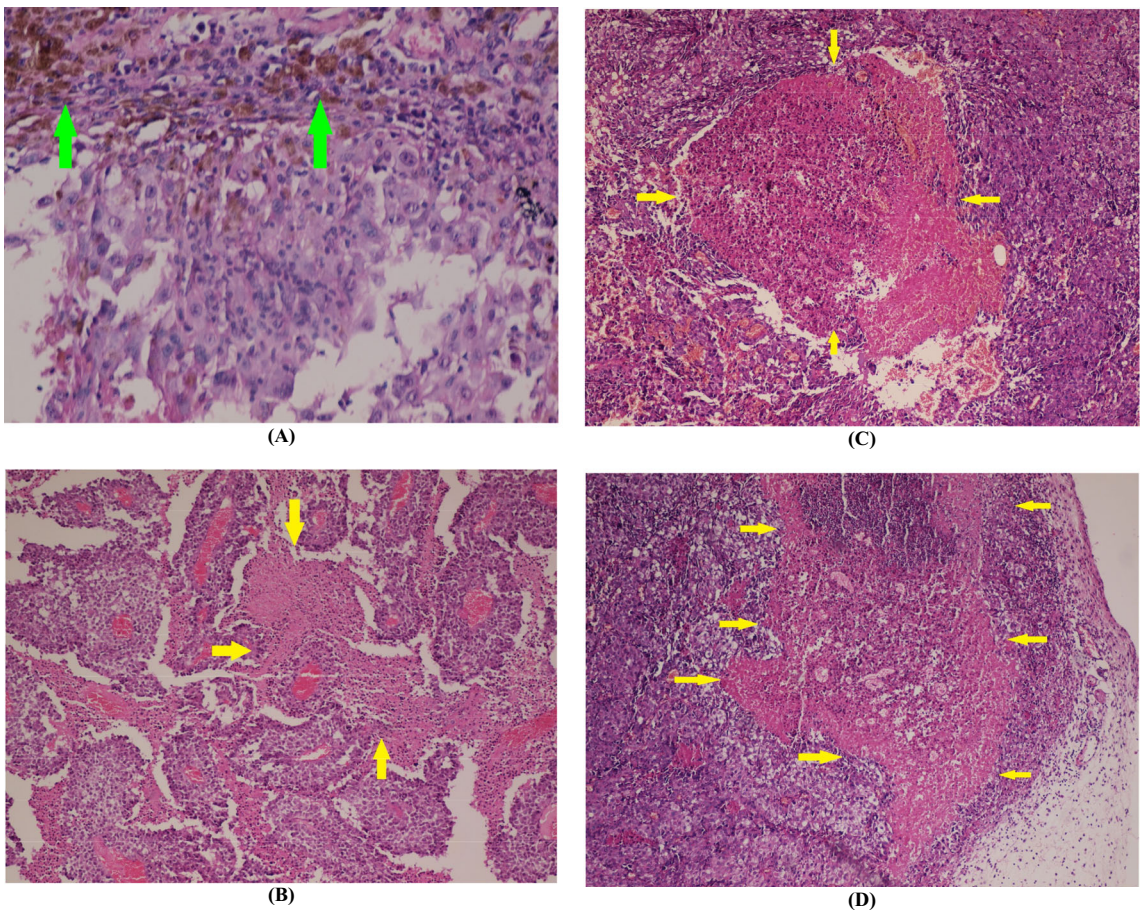

Fig. 5 **a** Images of H&E-stained slides (×400) of $L^{-}N^{-}_{mouse}$ group with viable malignant cells containing brownish melanin pigment (green arrows). **b** H&E-stained slide (×100) of the subject in $L^{+}N^{-}_{mouse}$ group with intermediate necrosis level. **c** H&E-stained slide (×100) of the subject in $L^{-}N^{+}_{mouse}$ group. **d** H&E-stained slide (×100) of the subject in $L^{+}N^{+}_{mouse}$ group. Yellow arrows show coagulative necrosis

melanoma tumor-bearing mice was examined in different groups. The tumor size of the mice in the four groups was measured before and 48 h after treatment. Figure 4 shows the tumor volume in the mouse groups upon treatment. Based on the obtained results, the solid tumors for the mice in the $L^{+}N^{+}_{mouse}$ group shrank and began to scab after 2 days with a considerable reduction in volume, while a rapid upward trend of tumor volume was observed in the $L^{-}N^{-}_{mouse}$, and the tumor growth in the $L^{+}N^{-}_{mouse}$ and $L^{-}N^{+}_{mouse}$ groups was inhibited. Therefore, administration of PEG-Cur-Au NPs or irradiation of 808-nm light alone inhibited the tumor growth rate, and their combination led to tumor treatment via PPT. This observation can be related to the dual effect of nanoparticles arising from chemotherapeutic role of curcumin and thermal destructive effect of GNPs grafted in PEG. It should also be added that in terms of appearance and general health, no loss in the mice body weight was observed in the $L^{-}N^{+}_{mouse}$ and $L^{+}N^{+}_{mouse}$ groups. Therefore, the photothermal therapy did not have a negative impact in physical health of the mice.

Efficacy of the photothermal therapy for destruction of malignant cells in four subject groups was also histologically evaluated. The animals were sacrificed 48 h after treatment. Both the treated and non-treated tumors were composed of one nodule that contained malignant melanoma cells with melanin pigments. After H&E staining, it was found that melanin pigment was in brown color images. Figure 5a–d shows images from the slides of H&E-stained tumor from the four groups. Figure 5a shows viable malignant cells with brown color melanin pigment in the tumor tissue (grade 1 necrosis, < 5%) in $L^{-}N^{-}_{mouse}$ group. Figure 5b shows a slide image of H&E-stained tumor from $L^{+}N^{-}_{mouse}$ group. It shows that treatment of tumors with laser radiation in the absence of the nanoparticles induced a mild coagulative necrosis in the tumor mass. Figure 5c shows the foci of coagulative tumor cell necrosis (grade three of necrosis) in the tumor area of the $L^{-}N^{+}_{mouse}$ group. Therefore, after injection of PEG-Cur-Au NPs in the tumor, a cytopathic effect occurred. Figure 5d shows images from H&E-stained slide of the tumor from the $L^{+}N^{+}_{mouse}$ group that was exposed to laser irradiation after nanoparticle injection. Tumor of the $L^{+}N^{+}_{mouse}$ group showed necrosis in grade 4 with a more necrosis accompanied with severe inflammation. Figure 6 indicates that no inflammation was shown in organs like kidney and liver, and they had a normal histology.

The uptake level of PEG-Cur-Au NPs by the cancer cells was determined by ICP-OES. Tumors of animals in the $L^{-}N^{+}_{mouse}$ group (received PEG-Cur-Au NPs of 2.5 mg mL^{-1}, 200 μL) which were sacrificed after 48 h post-injection were digested in aqua regia, and the gold concentration was determined. The results showed a level of 60 μg gold in each gram of tumor. The enhanced cytotoxicity

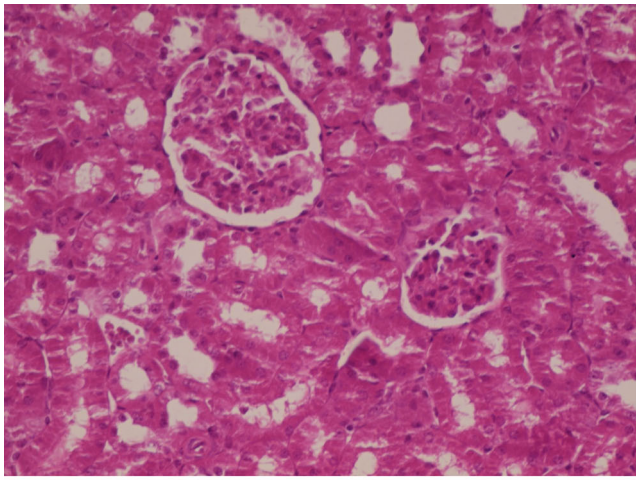

(A)

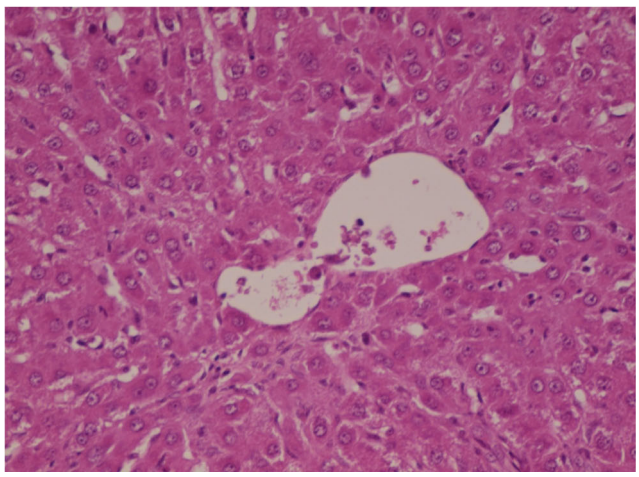

(B)

Fig. 6 H&E-stained slide (×400) of normal (**a**) kidney and (**b**) liver of subject in $L^{+}N^{+}_{mouse}$ group

effect of curcumin in tumor indicates entry of PEG-Cur-Au NPs into cells as confirmed with ICP-OES result.

Conclusion

In this study, we presented PEG-Cur-Au NPs as a novel NIR light activatable photothermal therapy agent. Photothermal outcome of the nanoparticles depends on their concentration and the power density of incoming laser light. PEG-Cur-Au NPs along with laser irradiation at 808 nm are able to destroy B16/F10 melanoma tumors. The photothermal efficacy of PEG-Cur-Au NPs arose from different mechanisms of enhancement in the solubility of curcumin by both PEG and GNP components, photodynamic effect of curcumin, and photothermal effect of GNPs. PEG-Cur-Au NPs can be introduced as a therapeutic agent with minimum invasive approach.

Acknowledgements This paper was extracted from F. Rahimi-Moghaddam M.Sc. thesis supported by the Research Council of Shiraz University of Medical Sciences (11648).

Compliance with ethical standards

Conflict of interest The authors declare that they have no conflict of interest.

Ethical approval This study was conducted according to the Committee on the Ethics of Animal Experiments of Shiraz University of Medical Sciences.

References

1. Zbytek B, Carlson JA, Granese J, Ross J, Mihm MC Jr, Slominski A (2008) Current concepts of metastasis in melanoma. Expert Rev Dermatol 3:569–585
2. Wyld L, Audisio RA, Poston GJ (2015) The evolution of cancer surgery and future perspectives. Nat Rev Clin Oncol 12:115–124
3. Moran MS (2015) Radiation therapy in the locoregional treatment of triple-negative breast cancer. Lancet Oncol 16:113–122
4. Deng GL, Zeng S, Shen H (2015) Chemotherapy and target therapy for hepatocellular carcinoma: new advances and challenges. World J Hepatol 7:787–798
5. Sahu A, Choi WI, Lee JH, Tae G (2013) Graphene oxide mediated delivery of methylene blue for combined photodynamic and photothermal therapy. Biomaterials 34:6239–6248
6. Mousavy SJ, Riazi GH, Kamarei M, Aliakbarian H, Sattarahmady N, Sharifizadeh A, Safarian S, Ahmad F, Moosavi-Movahedi AA (2009) Effects of mobile phone radiofrequency on the structure and function of the normal human hemoglobin. Int J Biol Macromol 44: 278–285
7. Shibu ES, Hamada M, Murase N, Biju V (2013) Nanomaterials formulations for photothermal and photodynamic therapy of cancer. J Photochem Photobiol C: Photochem Rev 15:53–72
8. Huang XH, El-Sayed IH, Qian W, El-Sayed MA (2006) Cancer cell imaging and photothermal therapy in the near-infrared region by using gold nanorods. J Am Chem Soc 128:2115–2120
9. Kubler C, Reuther T (2007) Photodynamic therapy. Possibilities and limits for head and neck carcinomas. Onkologe 13:158–164
10. Choi WI, Kim JY, Kang C, Byeon CC, Kim YH, Tae G (2011) Tumor regression in vivo by photothermal therapy based on gold-nanorod-loaded, functional nanocarriers. ACS Nano 5:1995–2003
11. Okuno T, Kato S, Hatakeyama Y, Okajima J, Maruyama S, Sakamoto M, Mori S, Kodama T (2013) Photothermal therapy of tumors in lymph nodes using gold nanorods and near-infrared laser light. J Control Release 172:879–884
12. Boca SC, Potara M, Gabudean AM, Juhem A, Baldeck PL, Astilean S (2011) Chitosan-coated triangular silver nanoparticles as a novel class of biocomptible, highly effective photothermal transducers for in vitro cancer cell therapy. Cancer Lett 311:131–140
13. Wang TT, Zhang LY, Su ZM, Wang CG, Liao Y, Fu Q (2011) Multifunctional hollow mesoporous silica nanocages for cancer cell detection and the combined chemotherapy and photodynamic therapy. ACS Appl Mater Interfaces 3:2479–2486
14. Tian QW, Tang MH, Sun YG, Zou RJ, Chen ZG, Zhu MF, Yang SP, Wang JL, Wang JH (2011) Hydrophilic flower-like CuS superstructures as an efficient 980 nm laser-driven photothermal agent for ablation of cancer cells. Adv Mater 23:3542–3547
15. Huang XQ, Tang SH, Mu XL, Dai Y, Chen GX, Zhou ZY, Ruan FX, Yang ZL, Zheng NF (2011) Free standing palladium nanosheets with plasmonic and catalytic properties. Nat Nanotechnol 6:28–32
16. Sattarahmady N, Rezaie-Yazdi M, Tondro GH, Akbari N (2017) Bactericidal laser ablation of carbon dots: an in vitro study on wild-type and antibiotic-resistant Staphylococcus aureus. J Photochem Photobiol B 166:323–332
17. Huang XH, Jain PK, El-Sayed IH, El-Sayed MA (2008) Plasmonic photothermal therapy (PPTT) using gold nanoparticles. Lasers Med Sci 23:217–228
18. Sattarahmady N, Tondro GH, Golchin M, Heli H (2015) Gold nanoparticles biosensor of Brucella spp. genomic DNA: visual and spectrophotometric detections. Biochem Eng J 97:1–7
19. Gad SC, Sharp KL, Montgomery C, Payne JD, Goodrich GP (2012) Evaluation of the toxicity of intravenous delivery of auroshell particles (gold-silica nanoshells). Int J Toxicol 31:584–594
20. Sattarahmady N, Rahi A, Heli H (2017) A signal-on built in-marker electrochemical aptasensor for human prostate-specific antigen based on a hairbrush-like gold nanostructure. Sci Rep 7:11238
21. Hu J, Sanz-Rodrigue F, Rivero F, Rivero EM, Torres RA, Ortgies DH, Sole JG, Alfonso F, Jaque D (2018) Gold nanoshells: contrast agents for cell imaging by cardiovascular optical coherence tomography. Nano Res 11:676–685
22. Moradi M, Sattarahmady N, Rahi A, Hatam GR, Sorkhabadi SMR, Heli H (2016) Label-free, PCR-free and signal-on electrochemical DNA biosensor for Leishmania major based on gold nanoleaves. Talanta 161:48–53
23. Dehdari Vais R, Sattarahmady N, Karimian K, Heli H (2015) Green electrodeposition of gold hierarchical dendrites of pyramidalnanoparticles and determination of azathioprine. Sensors Actuators B 215:113–118
24. Chen J, Liang H, Lin L, Guo ZP, Sun PJ, Chen MW, Tian HY, Deng MX, Chen XS (2016) Gold nanorods-based gene carriers with the capability of photoacoustic imaging and photothermal therapy. ACS Appl Mater Interfaces 8:31558–31566
25. Heidari M, Sattarahmady N, Azarpira N, Heli H, Mehdizadeh A, Zare T (2016) Photothermal cancer therapy by gold-ferrite nanocomposite and near-infrared laser in animal model. Lasers Med Sci 31:221–227
26. Kirui DK, Rey DA, Batt CA (2010) Gold hybrid nanoparticles for targeted phototherapy and cancer imaging. Nanotechnology 21: 105105
27. Qiu JJ, Wei WD (2014) Surface plasmon-mediated photothermal chemistry. J Phys Chem C 118:20735–20749
28. Sattarahmady N, Kayani Z, Heli H (2015) Highly simple and visual colorimetric detection of Brucella melitensis genomic DNA in clinical samples based on gold nanoparticles. J Iran Chem Soc 12: 1569–1576
29. Gamal-Eldeen AM, Moustafa D, El-Daly SM, El-Hussieny EA, Saleh S, Khoobchandani M, Bacon KL, Gupta S, Katti K, Shukla R, Katti KV (2016) Photothermal therapy mediated by gum Arabic-conjugated gold nanoparticles suppresses liver preneoplastic lesions in mice. J Photochem Photobiol B 163:47–56
30. Nakamura T, Tamura A, Murotani H, Oishi M, Jinji Y, Matsuishi K, Nagasaki Y (2010) Large payloads of gold nanoparticles into the polyamine network core of stimuli-responsive PEGylated nanogels for selective and noninvasive cancer photothermal therapy. Nano 2: 739–746
31. Abo-Elfadi MT, Gamal-Eldeen AM, Elshafey MM, Abdalla GM, Ali SS, Ali MRK, Zawrah ZMFM (2016) Photothermal therapeutic effect of PEGylated gold nano-semicubes in chemically-induced skin cancer in mice. J Photochem Photobiol B 164:21–29
32. Chen R, Zheng XC, Qian HQ, Wang X, Wang J, Jiang XQ (2013) Combined near-IR photothermal therapy and chemotherapy using

gold-nanorod/chitosan hybrid nanospheres to enhance the antitumor effect. Biomater Sci 1:285–293
33. Martins CVB, da Silva DL, Neres ATM, Magalhaes TFF, Watanabe GA, Modolo LV, Sabino AA, de Fatima A, de Resende MA (2009) Curcumin as a promising antifungal of clinical interest. J Antimicrob Chemother 63:337–339
34. Kuttan R, Bhanumathy P, Nirmala K, George MC (1985) Potential anticancer activity of turmeric (Curcuma longa). Cancer Lett 29: 197–202
35. Ribeiro APD, Pavarina AC, Dovigo LN, Brunetti IL, Bagnato VS, Vergani CE, Costa CAD (2013) Phototoxic effect of curcumin on methicillin-resistant Staphylococcus aureus and L929 fibroblasts. Lasers Med Sci 28:391–398
36. Paschoa MA, Tonon CC, Spolidorio DMP, Bagnato VS, Giusti JSM, Santos-Pinto L (2013) Photodynamic potential of curcumin and blue LED against Streptococcus mutans in a planktonic culture. Photodiagn Photodyn Ther 10:313–319
37. Choudhuri T, Pal S, Agwarwal ML, Das T, Sa G (2002) Curcumin induces apoptosis in human breast cancer cells through p53-dependent Bax induction. FEBS Lett 512:334–340
38. Javvadi P, Segan AT, Tuttle SW, Koumenis C (2008) The chemopreventive agent curcumin is a potent radiosensitizer of human cervical tumor cells via increased reactive oxygen species production and overactivation of the mitogen-activated protein kinase pathway. Mol Pharmacol 73:1491–1501
39. Liu HL, Chen Y, Cui GH, Zhou JF (2005) Curcumin, a potent antitumor reagent, is a novel histone deacetylase inhibitor regulating B-NHL cell line Raji proliferation. Acta Pharmacol Sin 26:603–609
40. Ahn JC, Kang JW, Shin JI, Chung PS (2012) Combination treatment with photodynamic therapy and curcumin induces mitochondria-dependent apoptosis in AMC-HN3 cells. Int J Oncol 41:2184–2190
41. Dujic J, Kippenberger S, Ramirez-Bosca A, Diaz-Alperi J, Bereiter-Hahn J, Kaufmann R, Bernd A, Hofmann M (2009) Curcumin in combination with visible light inhibits tumor growth in a xenograft tumor model. Int J Cancer 124:1422–1428
42. Wu WT, Shen J, Banerjee P, Zhou SQ (2011) Water-dispersible multifunctional hybrid nanogels for combined curcumin and photothermal therapy. Biomaterials 32:598–609
43. Dovigo LN, Pavarina AC, Ribeiro APD, Brunetti IL, Costa CAD, Jacomassi DP, Bagnato VS, Kurachi C (2011) Investigation of the photodynamic effects of curcumin against Candida albicans. Photochem Photobiol 87:895–903
44. Singh DK, Jagannathan R, Khandelwal P, Abraham PM, Poddar P (2013) In situ synthesis and surface functionalization of gold nanoparticles with curcumin and their antioxidant properties: an experimental and density functional theory investigation. Nano 5: 1882–1893
45. Manju S, Sreenivasan K (2012) Gold nanoparticles generated and stabilized by water soluble curcumin-polymer conjugate: blood compatibility evaluation and targeted drug delivery onto cancer cells. J Colloid Interface Sci 368:144–151
46. Palmal S, Maity AR, Singh BK, Basu S, Jana NR (2014) Inhibition of amyloid fibril growth and dissolution of amyloid fibrils by curcumin-gold nanoparticles. Chem Eur J 20:6184–6191
47. Gangwar RK, Dhumale VA, Kumari D, Nakate UT, Gosavi SW, Sharma RB, Kale SN, Datar S (2012) Conjugation of curcumin with PVP capped gold nanoparticles for improving bioavailability. Mater Sci Eng C 32:2659–2663
48. Bot A, Obrocea M, Marincola FM (eds) (2011) Cancer vaccines: from research to clinical practice. Taylor and Francis, p 271
49. Song CW, Park HJ, Lee CK, Griffin R (2005) Implications of increased tumor blood flow and oxygenation caused by mild temperature hyperthermia in tumor treatment. Int J Hyperth 21:761–767
50. Kaneti YV, Chen CY, Liu MS, Wang XC, Yang JL, Taylor RA, Jiang XC, Yu AB (2015) Carbon-coated gold nanorods: a facile route to biocompatible materials for photothermal applications. ACS Appl Mater Interfaces 7:25658–25668
51. Bush JA, Cheung KJJ, Li G (2001) Curcumin induces apoptosis in human melanoma cells through a Fas receptor/caspase-8 pathway independent of p53. Exp Cell Res 271:305–314
52. Anand P, Kunnumakkara AB, Newman RA, Aggarwal BB (2007) Bioavailability of curcumin: problems and promises. Mol Pharm 4(2007):807–818
53. Zeng XB, Leung AWN, Xia XS, Yu HP, Bai DQ, Xiang JY, Jiang Y, Xu CS (2010) Effect of blue light radiation on curcumin-induced cell death of breast cancer cells. Laser Phys 20:1500–1503
54. Link S, El-Sayed MA (2000) Shape and size dependence of radiative, non-radiative and photothermal properties of gold nanocrystals. Int Rev Phys Chem 19:409–453
55. Zharov VP, Galitovsky V, Viegas M (2003) Photothermal detection of local thermal effects during selective nanophotothermolysis. Appl Phys Lett 83:4897–4899
56. Zharov VP, Galitovskaya EN, Johnson C, Kelly T (2005) Synergistic enhancement of selective nanophotothermolysis with gold nanoclusters: potential for cancer therapy. Lasers Surg Med 37:219–226
57. Liao HW, Hafner JH (2005) Gold nanorod bioconjugates. Chem Mater 17:4636–4641
58. Maeda H, Fang J, Inutsuka T, Kitamoto Y (2003) Vascular permeability enhancement in solid tumor: various factors, mechanisms involved and its implications. Int Immunopharmacol 3:319–328